Uniform optical gain as a non-Hermitian control knob

A. Hashemi [1,2] K. Busch,[3,4] S. K. Ozdemir [5] and R. El-Ganainy[1,2,*]

[1]*Department of Physics, Michigan Technological University, Houghton, Michigan 49931, USA*
[2]*Henes Center for Quantum Phenomena, Michigan Technological University, Houghton, Michigan 49931, USA*
[3]*Humboldt-Universität zu Berlin, Institut für Physik, AG Theoretische Optik & Photonik, D-12489 Berlin, Germany*
[4]*Max-Born-Institut, 12489 Berlin, Germany*
[5]*Department of Engineering Science and Mechanics and Materials Research Institute, The Pennsylvania State University, University Park, Pennsylvania 16802, USA*

(Received 6 July 2022; revised 30 September 2022; accepted 22 November 2022; published 7 December 2022)

Non-Hermitian optics utilizes judicious engineering of the spatial and spectral distribution of gain and loss in order to tailor the behavior of photonic systems in ways that could not be achieved by modulating only the real part of the refractive index. In this respect, a question that has never been addressed is whether a uniform distribution of gain or loss can also lead to nontrivial non-Hermitian effects in linear systems, beyond just signal amplification or decay. Here, we investigate this problem and demonstrate that the application of uniform gain to a symmetric photonic molecule (PM) can reverse the optical energy distribution inside the structure. For a PM composed of two coupled resonators, this translates into changing the optical energy distribution inside the resonators. For a PM formed through scattering or defect-induced intermodal coupling in a ring resonator, the applied gain, despite being uniform and symmetric, can impose a strong chirality and switch the direction of light propagation from dominantly clockwise to dominantly counterclockwise. These predictions are confirmed by using both coupled mode formalism and full-wave finite-element simulations. Our work establishes a different direction in the field of non-Hermitian optics where interesting behavior can be engineered not only by unbalancing the non-Hermitian parameter but also by changing its average value—a feature that was overlooked in previous works.

DOI: 10.1103/PhysRevResearch.4.043169

I. INTRODUCTION

The past few decades have witnessed tremendous progress in our ability to control the propagation and trapping of light and its interaction with matter. These developments were largely enabled by specially designed and fabricated structures such as photonic crystals [1,2], metamaterials [3], whispering gallery resonators [4], and chaotic resonators [5], just to mention a few examples. While these systems feature very different wave-dynamic effects, they all rely on engineering mainly the real refractive index of the material. On the other hand, optical loss and gain have been traditionally treated at a different level, with the former considered a nuisance to be avoided and the latter used mainly for amplification. Despite early attempts to utilize loss and/or gain for tailoring optical pulse delay time in the context of slow and fast light [6], it was not until the introduction of parity-time ($\mathcal{PT}$) symmetry [7] in optics [8–12] that these non-Hermitian parameters acquired a different role as additional degrees of freedom for molding the flow of light and building a new generation of photonic devices with unique optical responses (see [13–17] for recent reviews). The basic insight brought by these works is that a judicious choice of the spatial distribution of gain, loss, or their combinations can lead to exotic effects such as the formation of exceptional points (non-Hermitian spectral singularities where two or more eigenvalues of a system and their corresponding eigenvectors coalesce) [11,15,18–20], unidirectional invisibility [21,22], and loss-induced lasing (and the reverse effect) [23–25]. Subsequent studies showed that tailoring the spectral distribution of loss can also lead to interesting results such as the ability to achieve wave mixing in the absence of phase matching [26–28]. In all these studies, gain or loss was applied only to a subspace (spatial or spectral) of the full system in a preselected manner to achieve a desired functionality. For instance, this strategy was recently employed to control the emission characteristics of random and chaotic lasers by engineering the gain profile such that its overlap with the desired lasing mode is maximized [29–33]. This example illustrates the utility of nonuniform gain as a knob that can be externally controlled by shaping the pump field. On the other hand, it is well known that uniform gain can lead to interesting behavior beyond light amplification when nonlinear effects are involved [34,35].

The wealth of these results may indicate that interesting effects in linear non-Hermitian systems arise only for

*Corresponding author: ganainy@mtu.edu

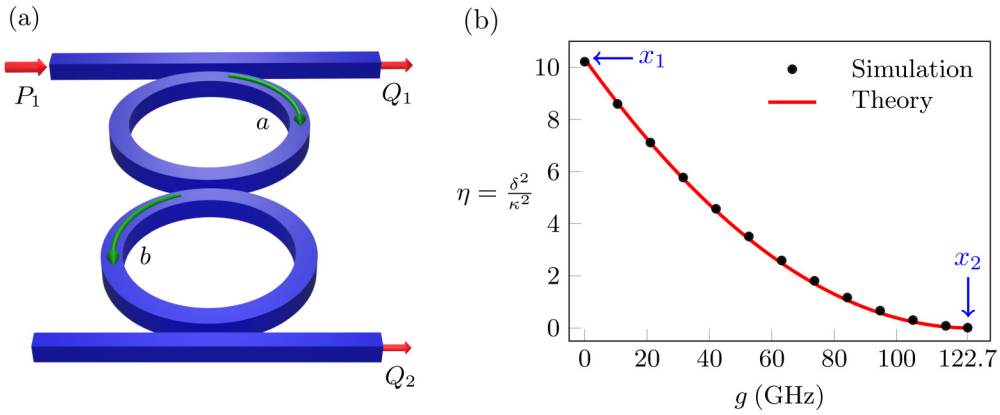

FIG. 1. (a) A schematic of a PM structure made of two coupled microcavities, together with two waveguide channels for excitation and collection, as indicated by the red arrows. In this example, we use microring resonators, but the analysis is valid for other types of resonators such as photonic crystals. (b) Plot of the asymmetry parameter $\eta \equiv |A/B|^2$, characterizing the ratio of the energy in resonator a to that of resonator b as a function of the homogeneous gain g under resonant condition $\Delta = 0$. The red solid line represents the results obtained by using the analytical formula indicated in the plot, while the black dots represent the results obtained with full-wave simulations. In applying the formula $\eta = \delta^2/\kappa^2$, we used the numerical values $\gamma = 123$ GHz and $\kappa = 39$ GHz, which are extracted from separate simulations, as discussed in Appendix A. All relevant parameters, such as the dimensions of the resonators and waveguides and refractive indices are given in Appendix A.

nonuniform distributions of gain and loss. With the exception of the recent work on active resonance [36], this narrative is supported by numerous studies of non-Hermitian optics, particularly those dealing with waveguide platforms. Consider, for instance, the first observation of $\mathcal{PT}$ symmetry breaking in a system of two coupled optical waveguides [37]. In that work, no gain was employed. Instead, one waveguide was almost transparent, while the other had an extra amount of loss (i.e., unbalanced loss profiles), creating a shifted $\mathcal{PT}$ system. This was possible because in waveguide setups, adding uniform gain shifts the complex eigenvalues (propagation constants) of both supermodes. This in turn leads to a net amplification effect without changing the propagation dynamics. The often invoked analogy between spatial and temporal coupled mode theories in waveguides and resonators has led to the assumption that similar behavior will occur in resonators and, consequently, to the implicit conclusion that nothing interesting can arise by using uniform gain in resonator systems, beyond signal amplification.

Here, we demonstrate that the aforementioned implication is, in fact, wrong. In particular, we show that the application of uniform gain to a photonic resonator system that harbors two spectrally close optical modes can have a profound impact on the system's response, beyond amplification effects. Specifically, we find that, under steady-state excitation from an external channel, the spatial distribution of the optical power inside the system depends on the value of the applied gain. We emphasize that this happens despite applying the gain uniformly across the entire structure without any spatial or spectral profile engineering. This remarkable effect in optical resonators is very different from the situation in waveguides where uniform gain provides only amplification without affecting the dynamics. This difference can be understood by noting that the analogy between spatial and temporal coupled mode theories is, in fact, incomplete. The former reduces the problem of coupled waveguides into linear coupled ordinary differential equations (ODEs) featuring an initial value problem. On the other hand, the latter describes coupled resonators by a system of coupled ODEs with additional driving terms and extra input/output equations. In other words, coupled optical resonators are driven-dissipative systems, while coupled waveguides are not. As we will see, it is this difference that leads to very distinct behavior in resonator systems.

II. RESULTS

We consider a generic photonic molecule (PM) structure [38,39] under steady-state excitation. PMs have attracted considerable attention recently because they can be used to engineer the linear spectrum of photonic structures and their associated field distributions for various applications such as sensing [40,41], frequency conversion [42], and optical comb generation [43]. For a comprehensive review of the spectral properties of PMs, see [44]. Figure 1(a) depicts one possible implementation of such a PM using microring resonators. Implementations using microdisk resonators or photonic crystal cavities are also possible. Later, we also discuss a different realization based on the coupling between counterpropagating waves in a single microring resonator.

The PM in Fig. 1(a) is excited from the top waveguide channel. An additional waveguide is added at the lower end in order to maintain the geometric symmetry of the structure. Measuring the optical energy inside the rings can be done either directly by using near-field measurements or indirectly by measuring the power at various output channels (e.g., outputs denoted as Q_1 and Q_2 in Fig. 1). Within the temporal coupled mode formalism [45], the above system is described by

$$i\frac{d\vec{v}}{dt} = H\vec{v} + i\sqrt{2\gamma}\vec{s}, \quad H = \begin{bmatrix} \omega_o - i\delta & \kappa \\ \kappa & \omega_o - i\delta \end{bmatrix}, \qquad (1)$$

where $\vec{v} = [a, b]$ represent the field components of the clockwise (CW) wave in resonator a and the counterclockwise (CCW) wave in resonator b. Here, ω_o is the bare resonant frequency of the degenerate CW and CCW modes of the

resonators in the absence of coupling, and $\delta = \gamma - g$ is a non-Hermitian parameter that accounts for material gain g and radiation loss through the waveguides γ. Throughout this work, we always assume that the system operates below the lasing threshold with $\delta > 0$. The parameter κ is the coupling coefficient introduced by the overlap between the evanescent fields of the resonators. Finally, the vector $\vec{s} = [s_1, 0]$ describes the excitation from port P_1, as indicated in Fig. 1(a). In the absence of any external excitations, the eigenvalues of the supermodes of this PM are given by $\mu_1 = \omega_o - i\delta - \kappa$ and $\mu_2 = \omega_o - i\delta + \kappa$, with the corresponding eigenvector given by $\vec{v}_{1,2} = [1, \mp 1]^T$. Let us turn the excitation from port P_1 on and assume it is a continuous wave at a frequency ω_o, i.e., $s_1 = s_o e^{-i\omega_o t}$. In this case, the steady-state field components inside the resonator, $[A, B]^T \equiv [a, b]^T e^{i\omega_o t}$, are given by

$$\vec{V} \equiv \begin{bmatrix} A \\ B \end{bmatrix} = \frac{\sqrt{2\gamma} s_o}{\delta^2 + \kappa^2} \begin{bmatrix} \delta \\ -i\kappa \end{bmatrix}. \tag{2}$$

Let us now define a parameter that quantifies the asymmetric power distribution between the CW and CCW modes $\eta \equiv |A/B|^2$. From Eq. (2), we find that $\eta = \delta^2/\kappa^2$. Clearly, the value of η can be controlled by varying κ. This is rather intuitive since κ is a measure of the coupling between the two modes of the resonators. What is surprising, however, is that the asymmetry parameter depends on δ and hence on the gain g even though it is applied equally to both resonators. As an illustrative example, assume that the design parameters are set to $\gamma = 5\kappa$ and $g = 0$ (i.e., initially there is no gain). In this case, we find $\eta = 25$, implying that optical power predominantly resides in the CW of resonator a. By applying a material gain (through optical or electrical pumping depending on the gain medium of the resonators) such that $\delta = \kappa$, we obtain $\eta = 1$ (i.e., optical energy is equally shared between the CW mode of resonator a and the CCW mode of the resonator b). Even more intriguing, by adjusting the applied gain value such that $\delta = \kappa/5$, we find $\eta = 0.04$, with most of the energy now residing in the CCW mode of resonator b. These results are rather counterintuitive as they demonstrate that one can control the asymmetric response of the system by using a symmetric knob.

We verify these results by performing full-wave simulations for the structure shown in Fig. 1(a) under different conditions. The geometry is chosen such that for the passive device we have $\gamma = 123$ GHz, $\kappa = 39$ GHz. The details of these simulations are discussed in Appendix A. Figures 2(a) and 2(b) depict the steady-state field distribution when $g = 0$ and $g = 122.7$ GHz, respectively. It is clearly seen that when no gain is applied, the energy mostly resides in resonator a. However, application of uniform optical gain (i.e., the same gain in both resonators) redistributes the energy to reside mainly in resonator b. Figure 1(b) plots the power asymmetry parameter η as a function of the uniform gain g and compares the predictions obtained from the Coupled Mode Theory (CMT) (red curve) to those obtained using full-wave simulations (black dots), where a near-perfect agreement between them is observed.

A second example that demonstrates the counterintuitive result of applying uniform gain in photonic molecules is depicted in Fig. 3(a). Here, we use only one microring resonator

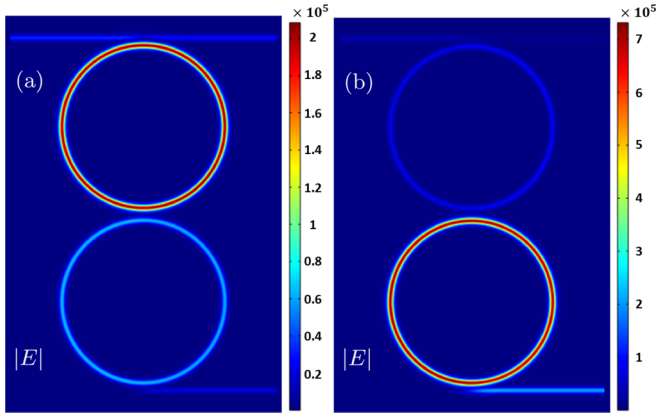

FIG. 2. Steady-state electric field distribution in a PM structure similar to that depicted in Fig. 1(a) under excitation from port P_1 when (a) no gain is applied [i.e., when the system is passive, which corresponds to point x_1 with $g = 0$ GHz in Fig. 1(b)] and (b) both cavities experience uniform gain of $g = 122.7$ GHz, corresponding to point x_2 in Fig. 1(b). In (a), optical energy dominantly resides in resonator a with $\eta = 10.2$, whereas in (b) the energy mostly resides in resonator b with $\eta = 0.01$. In other words, the application of uniform gain has reversed the optical response of the PM. In all simulations, the single resonator loss through the waveguide channel is $\gamma = 123$ GHz, which guarantees that the system operates below the lasing threshold. All the geometric and optical parameters associated with the simulations are listed in Appendix A.

and introduce coupling between its CW and CCW modes via a nanoscatterer (particle or notch, etc.) [46]. One can think of this system as a PM implemented using synthetic dimensions. From a mathematical point of view, this configuration is described by the same system of equations as in Eq. (1), except that the Hamiltonian must be modified to read

$$i\frac{d\vec{v}}{dt} = H\vec{v} + i\sqrt{2\gamma}\vec{s},$$
$$H = \begin{bmatrix} \omega_o - i\delta_p + \kappa_p & \kappa_p \\ \kappa_p & \omega_o - i\delta_p + \kappa_p \end{bmatrix}, \tag{3}$$

with $\delta_p = 2\gamma - g$ (since now each mode experiences loss via both waveguides). The additional κ_p factor on the diagonal elements accounts for the fact that the scatterer also shifts the frequencies of the individual modes. In this case, the eigenvalues of the supermodes are given by $\mu_1 = \omega_o - i\delta_p$ and $\mu_2 = \omega_o - i\delta_p + 2\kappa_p$; that is, one eigenfrequency remains unchanged, while the other is shifted by $2\kappa_p$. This picture is consistent with the field distribution associated with this situation where the introduction of the scatterer results in two standing wave modes: One that exhibits a null field at the scatterer location and thus is not affected by its presence and one that exhibits a peak field value at the scatterer and thus experiences a maximum frequency shift. One can thus follow exactly the same analysis as before by using the field components $\vec{v}_s = [a_{CW}, a_{CCW}]^T$ and $\vec{V}_s = [A_{CW}, A_{CCW}]^T$ and the excitation $s_1 = s_o e^{-i(\omega_o + \kappa_p)t}$ to obtain $\eta_p \equiv |A_{CW}/A_{CCW}|^2 = \delta_p^2/\kappa_p^2$. In other words, by varying the uniform gain parameter g, one can switch the chiral response of the microring from predominantly CW to predominantly CCW. These results are confirmed by using full-wave analysis, as shown in Fig. 3(b)

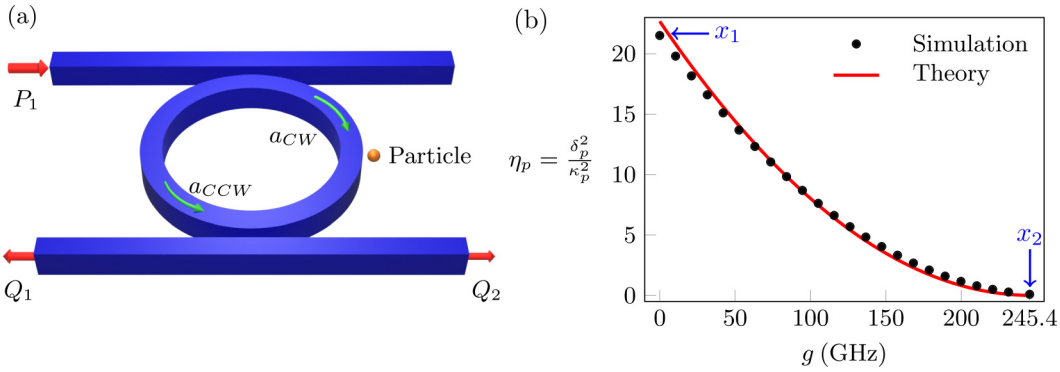

FIG. 3. (a) A schematic representation of a PM formed by using a two-dimensional synthetic dimension spanned by frequency-degenerate propagating CW and CCW modes in a ring resonator, where the coupling between the modes is introduced via a nanoscatterer. Here, the excitation channel is P_1, and the collection channels are Q_1 and Q_2. (b) Plot of the parameter η_p with respect to the gain parameter g under resonant condition $\Delta = 0$. The red solid line depicts the plot of results obtained from CMT for $\eta_p = \delta_p^2/\kappa_p^2$ when $\gamma = 123$ GHz and $\kappa_p = 52$ GHz, while the black dots represent the results of the full-wave simulations. All the geometric and optical parameters associated with the simulations are listed in Appendix A.

for the η_p-g plot as well as Figs. 4(a) and 4(b) for the field distribution. Beyond the intriguing aspect of these results, they indicate that one must exercise extreme caution when constructing the properties of any system by examining its response. For instance, in the above example, the regime $\eta = 1$ can be very misleading since naively looking at the output from the lower waveguide, one could be tempted to conclude that the excitation is symmetric, which is obviously wrong. We also note that the situation we observe here is different from the reversal of chirality (rotation direction of light) in a whispering-gallery-mode resonator demonstrated in [47]. While in that work chirality reversal is achieved by moving the system from one exceptional point to another, here, chirality reversal is achieved by the application of uniform gain, and exceptional points are not involved.

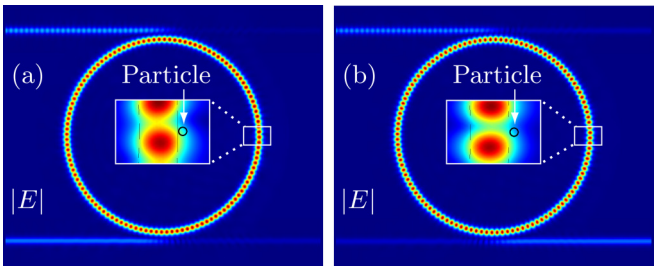

FIG. 4. Steady-state electric field distribution in a PM structure similar to that depicted in Fig. 3(a) under excitation from port P_1 when (a) no gain is applied [i.e., under passive conditions corresponding to point x_1 in Fig. 3(b)] and 3(b) a uniform gain of $g = 245.4$ GHz is applied, which corresponds to point x_2 in Fig. 3(b). In the first case, only 4% of the intracavity optical energy resides in the CCW mode, as evidenced by the output power from the two ports of the lower waveguide, while in the second scenario most of the energy (∼92%) populates the same CCW mode, and hence, more output power travels through the right channel of the lower waveguide. In all simulations, the resonator loss through each waveguide channel is $\gamma = 123$ GHz with the total loss given by 2γ, thus ensuring operation below the lasing threshold. All the geometric and optical parameters associated with the simulations are listed in Appendix A.

Having demonstrated that the application of a uniform gain can have a profound effect on the optical power distribution inside PMs, we may wonder about the physical mechanism responsible for these interesting results. At first sight, it may appear that any change in the value of the asymmetry coefficient is a result of exciting different weights of the eigenvectors $\vec{v}_{1,2} = [1, \pm 1]^T$. This, however, is not the case. In fact, regardless of the design parameters, the two vectors are always excited with equal magnitudes. In order to understand the reason for this interesting behavior, we return to Eq. (2), which is associated with Fig. 1(a) [one can make the same argument about the example shown in Fig. 3(a)] and describes the steady-state complex field amplitudes inside the resonators, and reexpress it in terms of the eigenvectors to obtain

$$\vec{V} = \frac{\sqrt{2\gamma}s_o}{2\sqrt{\delta^2+\kappa^2}}\left\{e^{-i\phi}\vec{v}_1 + e^{i\phi}\vec{v}_2\right\} = \frac{\sqrt{2\gamma}s_o}{\sqrt{\delta^2+\kappa^2}}\begin{bmatrix}\cos\phi \\ -i\sin\phi\end{bmatrix}, \tag{4}$$

where $\phi = \arctan(\kappa/\delta)$. Expressed in terms of the angle ϕ, the asymmetric parameter reads $\eta = \cot^2\phi$. Thus, apart from a general scaling prefactor that determines the total energy inside the resonator, it is the phase ϕ that dictates the degree of asymmetry in energy distribution between the two sites or the two modes. This phase factor depends on the excitation frequency relative to the two eigenfrequencies of the supermodes but also on the relative linewidth of these modes, which in turn is a function of the applied gain.

III. CONCLUSION

In this work, we have demonstrated that uniform gain or loss distribution in linear non-Hermitian optical setups can have a significant impact on the system's response beyond the trivial effect of power amplification or dissipation. In particular, we show that the application of uniform gain to a symmetric PM can totally alter the optical energy distribution inside the structure. We have illustrated our results for PMs made of two coupled microresonators and for a PM formed by the coupling between internal modes of a

single microresonators. Our results, which were obtained via temporal coupled mode theory, are also confirmed by performing full-wave simulations of Maxwell's equations using silicon photonic material systems. Importantly, we note that in contrast to earlier studies on controlling laser emission by engineering the refractive index profile (see, for example, [48,49]) and the recent work demonstrating that, under linear conditions, an intricate correlation between uniform gain and a very special parabolic index distribution (with vanishing value at the center of the structure) can give rise to a novel active resonance [36], the results reported in this work do not rely on engineering the relation between the gain and refractive index. In addition, in our work, uniform gain acts as a continuous tuning parameter. To further emphasize these findings, we have checked that our results indeed extend to larger systems such as those made of three coupled resonators, as we demonstrate in Appendix B.

These results raise some important questions. For instance, several recent studies investigated localization properties in disordered non-Hermitian waveguide arrays [50,51] which fall into the class of initial value problems. In that case, the average value of the gain does have a trivial impact on the outcome; namely, it acts as an amplification factor. Our work here indicates that the situation could be very different in a system of a disordered driven-dissipative coupled resonator. In particular, the relationship between wave localization and transport properties in driven-dissipative systems under variation of average loss (or gain) values is not at all clear. Another interesting question is whether one can devise optical systems whose topological features can be controlled by applying uniform gains. We plan to investigate these problems in future works.

ACKNOWLEDGMENTS

This work is supported by the Air Force Office of Scientific Research (AFOSR) Multidisciplinary University Research Initiative (MURI) Award on Programmable systems with non-Hermitian quantum dynamics (Award No. FA9550-21-1-0202). R.E.-G. also acknowledges support from NSF (Grant No. ECCS 1807552) and the Alexander von Humboldt Foundation. S.K.O. also acknowledges support from NSF (Grant No. ECCS 1807485). K.B. acknowledges support from the Leibniz Association within the SAW project LAPTON and from the Alexander von Humboldt Foundation. K.B. and R.E. acknowledge support from the Deutsche Forschungsgemeinschaft (DFG), SFB 951 (Project No. 182087777).

APPENDIX A: NUMERICAL EVALUATION OF THE OPTICAL PARAMETERS

In this Appendix, we present the simulation details. In what follows, all the simulations are performed using the full-wave finite-element method (using the COMSOL commercial software package) by assuming two-dimensional geometries. For the structure shown in Fig. 1(a), the simulation parameters were chosen as follows: The outer radii of both microring resonators are $R = 5$ μm, the ring waveguide widths (which are also identical to the widths of the waveguide channels) are $w = 0.25$ μm, and the edge-to-edge separation between each ring and its adjacent waveguide is $d_1 = 0.2$ μm, while the edge-to-edge separation between the two rings is $d_2 = 0.5$ μm. The refractive indices of the microring resonators and waveguides are taken to be $n_r = 3.47$ and are assumed to be embedded in a background with a refractive index of $n_b = 1.44$. These values are relevant to the standard silicon photonics platform. Among the many modes supported by this structure, we focus on the resonant TE modes with frequency $\omega_o = 1217\times10^9$ rad s^{-1}(or, equivalently, $\lambda_o = 1548$ nm) and an effective refractive index of $n_{\text{eff}} = 2.93$.

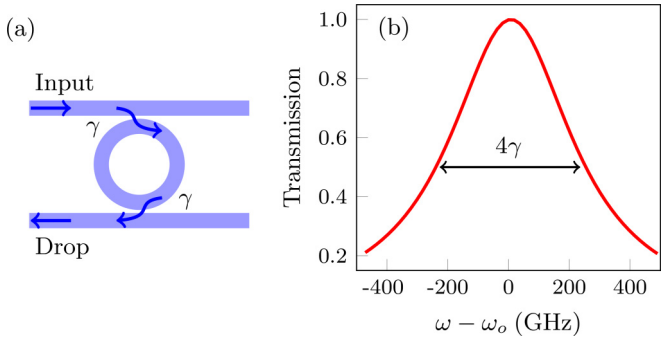

FIG. 5. An add-drop setup with one ring resonator is used to evaluate the dissipation coefficient γ through the width of the transmission spectrum at the half of its maximum value. In this simulation $\gamma = 123$ GHz is obtained.

The numerical value of the dissipation coefficients γ is evaluated by using an add-drop filter configuration in the absence of gain, as shown in Fig. 5(a) (see [52] for details). By doing so and plotting the transmission as a function of frequency detuning [Fig. 5(b)], we obtain $\gamma = 123$ GHz.

Next, we consider a two-ring add-drop configuration as shown in Fig. 6 in order to evaluate the coupling coefficient κ between the two rings. In this case, it is straightforward to derive an expression for P_{drop} in terms of the parameters associated with the temporal coupled mode theory:

$$P_{\text{drop}} \equiv \left|\frac{Q_2}{s}\right|^2 = \frac{4\gamma^2\kappa^2}{\Delta^4 + 2\Delta^2(\gamma^2-\kappa^2) + (\gamma^2+\kappa^2)^2}, \quad \text{(A1)}$$

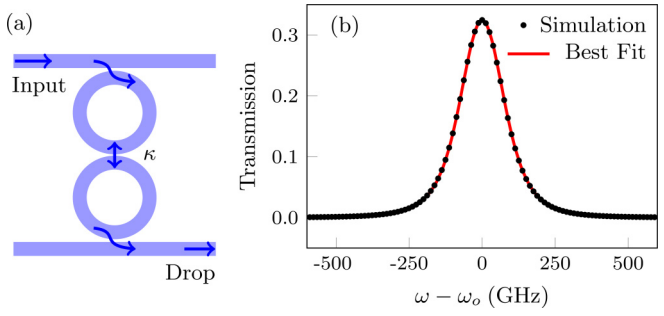

FIG. 6. (a) An add-drop configuration is considered to determine the numerical value of the ring-ring coupling coefficient κ. This platform does not have any gain. (b) The input signal is launched from the input port, and the normalized power transmission from the drop port is depicted with respect to the frequency detuning. By fitting the simulation data for the power transmission with the theoretical expression in (A1), we obtained $\kappa = 39$ GHz.

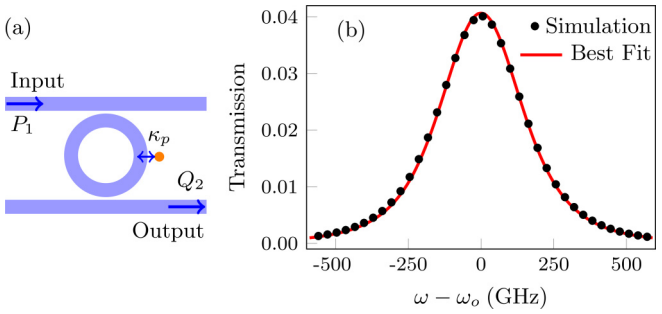

FIG. 7. (a) Schematic of the geometry used to evaluate the ring-particle coupling coefficient κ_p. This platform does not have any gain. (b) The input signal is driven from the input port, and the normalized power transmission is measured through the output port. By fitting the simulation data (black dotted curve) with the theoretical result in Eq. (A2), we obtained $\kappa_p = 52$ GHz.

where $|Q_2|^2$ is the output power from the drop port, $\Delta \equiv \omega - \omega_o$ is the frequency detuning, and $|s|^2$ is the input power.

The black dots in Fig. 6(b) present the actual normalized drop power data obtained from full-wave simulations. By performing curve fitting between these data points and the expression in (A1), we obtain $\kappa = 39$ GHz. These values of γ and κ are then used to compare the results obtained from coupled mode analysis and full-wave simulations. In the latter case, gain is introduced through the imaginary part of the refractive index n_i by considering $g = -\omega_o(n_i/n_r)$, with gain corresponding to a negative value of n_i.

For the structure shown in Fig. 3(a), the parameters of the ring and waveguide are identical to those used above. The radius and refractive index for the nanoparticle are taken to be $r = 30$ nm and $n_p = 3.5$, while its location is chosen to be centered at the distance $d_p = 32$ nm from the circumference of the ring in a symmetric position with respect to the two waveguides [see Fig. 3(a)]. In addition to the coupled mode parameters obtained before, here, we need also to obtain the numerical value of the coupling between the CW and CCW modes due to the presence of the particle. To do so, we perform a full-wave simulation for the configuration shown in Fig. 7(a) and plot the normalized transmission as a function of the input signal frequency, as shown in Fig. 7(b). By fitting these results to the theoretical expression obtained by using coupled mode theory,

$$P_{Q_2} \equiv \left|\frac{Q_2}{s}\right|^2 = \frac{4\gamma^2\kappa_p^2}{\Delta^4 + 2\Delta^2\left(4\gamma^2 - \kappa_p^2\right) + \left(4\gamma^2 + \kappa_p^2\right)^2} \quad \text{(A2)}$$

we obtain $\kappa_p = 52$ GHz.

From these same simulations, we also obtain the parameter $\eta_s = |Q_1/Q_2|^2$.

APPENDIX B: THREE COUPLED RESONATORS

In this Appendix, we check whether our results still hold for larger systems. To do so, we consider a structure that consists of three coupled ring resonators, as shown in Fig. 8(a). Within the context of temporal coupled mode theory, this structure is modeled by the Hamiltonian matrix:

$$H = \begin{bmatrix} \omega_o - i\delta & \kappa & 0 \\ \kappa & \omega_o + ig & \kappa \\ 0 & \kappa & \omega_o - i\delta \end{bmatrix}, \quad \text{(B1)}$$

where, as before, $\delta = \gamma - g$. The eigenvalues of H and the corresponding eigenvectors are given by $\mu_1 = \omega_o - i\delta$, $\mu_{2,3} = \omega_o + i(g - \frac{\gamma}{2}) \pm \frac{1}{2}\sqrt{8\kappa^2 - \gamma^2}$ and $v_1 = [1, 0, -1]^T$, $v_{2,3} = [1, \frac{i\gamma \pm \sqrt{8\kappa^2 - \gamma^2}}{2\kappa}, 1]^T$, respectively. The system's response to a continuous wave excitation from port P_1 with a frequency ω_o is given by

$$\vec{V}_3 \equiv \begin{bmatrix} a_1 \\ a_2 \\ a_3 \end{bmatrix} = \frac{\sqrt{2\gamma}s_o e^{-i\omega_o t}}{\delta(g^2 + 2\kappa^2 - \gamma g)} \begin{bmatrix} \kappa^2 - \delta g \\ -i\kappa\delta \\ -\kappa^2 \end{bmatrix}, \quad \text{(B2)}$$

where a_j is the electric field amplitude in resonator j. From the above formula, it is clear that the value of the uniform gain (i.e., gain applied equally to all cavities) controls the ratio of the field amplitudes in the three sites. To better illustrate this behavior, we plot $\eta_3 \equiv |a_1/a_3|^2$ as a function of the applied gain, as shown in Fig. 8(b). These results confirm that the main conclusion of our work still holds for larger systems involving more than two interacting modes.

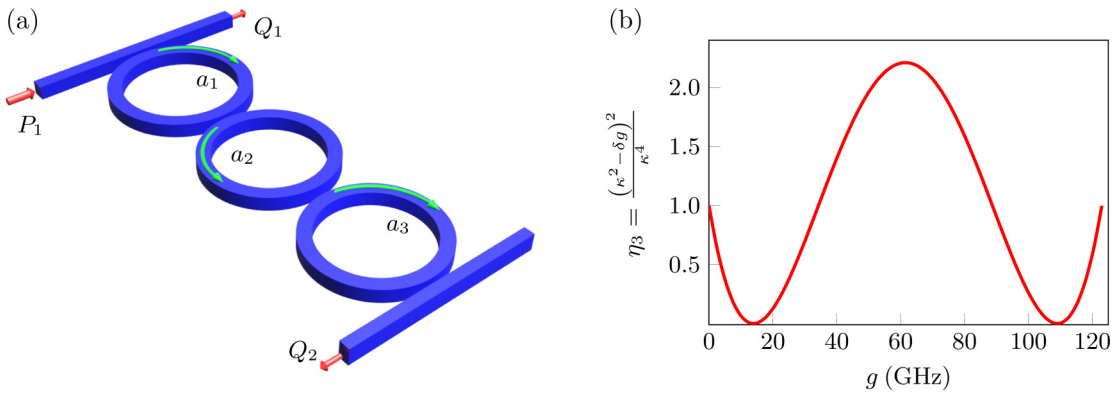

FIG. 8. (a) A schematic of an optical system consisting of three coupled ring resonators. (b) Plot of the asymmetry parameter $\eta_3 \equiv |a_1/a_3|^2 = (\kappa^2 - \delta g)^2/\kappa^4$ (with $\delta = \gamma - g$) as a function of the applied gain for $\kappa = 39$ (GHz) and $\gamma = 123$ (GHZ).

[1] J. D. Joannopoulos, S. G. Johnson, J. N. Winn, and R. D. Meade, *Photonic Crystals: Molding the Flow of Light* (Princeton University Press, Princeton, NJ, 2011).

[2] K. Busch, G. von Freymann, S. Linden, S. F. Mingaleev, L. Tkeshelashvili, and M. Wegener, Periodic nanostructures for photonics, Phys. Rep. **444**, 101 (2007).

[3] K. Sakoda, *Electromagnetic Metamaterials: Modern Insights into Macroscopic Electromagnetic Fields* (Nature Singapore Pte Ltd., 2019).

[4] F. Vollmer and D. Yu, *Optical Whispering Gallery Modes for Biosensing: From Physical Principles to Applications* (Springer Nature Switzerland AG, 2020).

[5] S. Aberg and K.-F. Berggren, *Quantum Chaos Y2K: Proceedings of Nobel Symposium 116* (World Scientific, Singapore, 2001).

[6] P. W. Milonni, *Fast Light, Slow Light and Left-Handed Light* (CRC Press, Boca Raton, FL, 2020).

[7] C. M. Bender and S. Boettcher, Real Spectra in non-Hermitian Hamiltonians Having $\mathcal{PT}$ Symmetry, Phys. Rev. Lett. **80**, 5243 (1998).

[8] R. El-Ganainy, K. G. Makris, D. N. Christodoulides, and Z. H. Musslimani, Theory of coupled optical pt-symmetric structures, Opt. Lett. **32**, 2632 (2007).

[9] Z. H. Musslimani, K. G. Makris, R. El-Ganainy, and D. N. Christodoulides, Optical Solitons in $\mathcal{PT}$ Periodic Potentials, Phys. Rev. Lett. **100**, 030402 (2008).

[10] K. G. Makris, R. El-Ganainy, D. N. Christodoulides, and Z. H. Musslimani, Beam Dynamics in $\mathcal{PT}$ Symmetric Optical Lattices, Phys. Rev. Lett. **100**, 103904 (2008).

[11] C. E. Rüter, K. G. Makris, R. El-Ganainy, D. N. Christodoulides, M. Segev, and D. Kip, Observation of parity-time symmetry in optics, Nat. Phys. **6**, 192 (2010).

[12] B. Peng, S. K. Özdemir, F. Lei, F. Monifi, M. Gianfreda, G. L. Long, S. Fan, F. Nori, C. M. Bender, and L. Yang, Parity-time-symmetric whispering-gallery microcavities, Nat. Phys. **10**, 394 (2014).

[13] L. Feng, R. El-Ganainy, and L. Ge, Non-Hermitian photonics based on parity–time symmetry, Nat. Photon. **11**, 752 (2017).

[14] R. El-Ganainy, K. Makris, Z. H. Khajavikhan, S. Rotter, and D. N. Christodoulides, Non-Hermitian physics and pt symmetry, Nat. Phys. **14**, 11 (2018).

[15] R. El-Ganainy, M. Khajavikhan, D. N. Christodoulides, and S. K. Özdemir, The dawn of non-Hermitian optics, Commun. Phys. **2**, 37 (2019).

[16] M.-A. Miri and A. Alu, Exceptional points in optics and photonics, Science **363**, 363 (2019).

[17] Ş. K. Özdemir, S. Rotter, F. Nori, and L. Yang, Parity–time symmetry and exceptional points in photonics, Nat. Mater. **18**, 783 (2019).

[18] J. Wiersig, Enhancing the Sensitivity of Frequency and Energy Splitting Detection by Using Exceptional Points: Application to Microcavity Sensors for Single-Particle Detection, Phys. Rev. Lett. **112**, 203901 (2014).

[19] J. Wiersig, Sensors operating at exceptional points: General theory, Phys. Rev. A **93**, 033809 (2016).

[20] A. Hashemi, S. M. Rezaei, S. K. Özdemir, and R. El-Ganainy, New perspective on chiral exceptional points with application to discrete photonics, APL Photon. **6**, 040803 (2021).

[21] Z. Lin, H. Ramezani, T. Eichelkraut, T. Kottos, H. Cao, and D. N. Christodoulides, Unidirectional Invisibility Induced by $\mathcal{PT}$-Symmetric Periodic Structures, Phys. Rev. Lett. **106**, 213901 (2011).

[22] L. Feng, Y.-L. Xu, W. S. Fegadolli, M.-H. Lu, J. E. B. Oliveira, V. R. Almeida, Y.-F. Chen, and A. Scherer, Experimental demonstration of a unidirectional reflectionless parity-time metamaterial at optical frequencies, Nat. Mater. **12**, 108 (2013).

[23] B. Peng, S. K. Özdemir, S. Rotter, H. Yilmaz, M. Liertzer, F. Monifi, C. M. Bender, F. Nori, and L. Yang, Loss-induced suppression and revival of lasing, Science **346**, 328 (2014).

[24] M. Brandstetter, M. Liertzer, C. Deutsch, P. Klang, J. Schöberl, H. E. Türeci, G. Strasser, K. Unterrainer, and S. Rotter, Reversing the pump dependence of a laser at an exceptional point, Nat. Commun. **5**, 4034 (2014).

[25] R. El-Ganainy, M. Khajavikhan, and L. Ge, Exceptional points and lasing self-termination in photonic molecules, Phys. Rev. A **90**, 013802 (2014).

[26] R. El-Ganainy, J. I. Dadap, and R. M. Osgood, Optical parametric amplification via non-Hermitian phase matching, Opt. Lett. **40**, 5086 (2015).

[27] Q. Zhong, A. Ahmed, J. I. Dadap, R. M. Osgood, Jr., and R. El-Ganainy, Parametric amplification in quasi-PT symmetric coupled waveguide structures, New J. Phys. **18**, 125006 (2016).

[28] A. Ahmed, X. Meng, Q. Zhong, R. El-Ganainy, R. M. Osgood, and J. I. Dadap, On-chip non-Hermitian optical parametric amplifiers with a large bandwidth, J. Opt. Soc. Am. B **38**, 2160 (2021).

[29] N. Bachelard, J. Andreasen, S. Gigan, and P. Sebbah, Taming Random Lasers through Active Spatial Control of the Pump, Phys. Rev. Lett. **109**, 033903 (2012).

[30] T. Hisch, M. Liertzer, D. Pogany, F. Mintert, and S. Rotter, Pump-Controlled Directional Light Emission from Random Lasers, Phys. Rev. Lett. **111**, 023902 (2013).

[31] N. Bachelard, S. Gigan, X. Noblin, and P. Sebbah, Adaptive pumping for spectral control of random lasers, Nat. Phys. **10**, 426 (2014).

[32] S. F. Liew, L. Ge, B. Redding, G. S. Solomon, and H. Cao, Pump-controlled modal interactions in microdisk lasers, Phys. Rev. A **91**, 043828 (2015).

[33] A. Cerjan, B. Redding, L. Ge, S. F. Liew, H. Cao, and A. D. Stone, Controlling mode competition by tailoring the spatial pump distribution in a laser: A resonance-based approach, Opt. Express **24**, 26006 (2016).

[34] M. Sorel, G. Giuliani, A. Scire, R. Miglierina, S. Donati, and P. J. R. Laybourn, Operating regimes of GaAs-AlGaAs semiconductor ring lasers: Experiment and model, IEEE J. Quantum Electron. **39**, 1187 (2003).

[35] Q.-T. Cao, H. Wang, C.-H. Dong, H. Jing, R.-S. Liu, X. Chen, L. Ge, Q. Gong, and Y.-F. Xiao, Experimental Demonstration of Spontaneous Chirality in a Nonlinear Microresonator, Phys. Rev. Lett. **118**, 033901 (2017).

[36] J. D. H. Rivero, M. Pan, K. G. Makris, L. Feng, and L. Ge, Non-Hermiticity-Governed Active Photonic Resonances, Phys. Rev. Lett. **126**, 163901 (2021).

[37] A. Guo, G. J. Salamo, D. Duchesne, R. Morandotti, M. Volatier-Ravat, V. Aimez, G. A. Siviloglou, and D. N. Christodoulides, Observation of $\mathcal{PT}$-Symmetry Breaking in Complex Optical Potentials, Phys. Rev. Lett. **103**, 093902 (2009).

[38] M. Bayer, T. Gutbrod, J. P. Reithmaier, A. Forchel, T. L. Reinecke, P. A. Knipp, A. A. Dremin, and V. D. Kulakovskii,

Optical Modes in Photonic Molecules, Phys. Rev. Lett. **81**, 2582 (1998).

[39] B. Peng, Ş. K. Özdemir, J. Zhu, and L. Yang, Photonic molecules formed by coupled hybrid resonators, Opt. Lett. **37**, 3435 (2012).

[40] S. V. Boriskina, Spectrally engineered photonic molecules as optical sensors with enhanced sensitivity: A proposal and numerical analysis, J. Opt. Soc. Am. B **23**, 1565 (2006).

[41] S. V. Boriskina and L. D. Negro, Self-referenced photonic molecule bio(chemical)sensor, Opt. Lett. **35**, 2496 (2010).

[42] M. Soltani, M. Zhang, C. Ryan, G. J. Ribeill, C. Wang, and M. Loncar, Efficient quantum microwave-to-optical conversion using electro-optic nanophotonic coupled resonators, Phys. Rev. A **96**, 043808 (2017).

[43] Ó. B. Helgason, F. R. Arteaga-Sierra, Z. Ye, K. Twayana, P. A. Andrekson, M. Karlsson, J. Schröder, and V. Torres-Company, Dissipative solitons in photonic molecules, Nat. Photon. **15**, 305 (2021).

[44] S. V. Boriskina, Photonic molecules and spectral engineering, in *Photonic Microresonator Research and Applications*, edited by I. Chremmos, O. Schwelb, and N. Uzunoglu (Springer, Boston, 2010), pp. 393–421.

[45] S. Fan, W. Suh, and J. D. Joannopoulos, Temporal coupled-mode theory for the Fano resonance in optical resonators, J. Opt. Soc. Am. A **20**, 569 (2003).

[46] J. Zhu, S. K. Ozdemir, Y.-F. Xiao, L. Li, L. He, D.-R. Chen, and L. Yang, On-chip single nanoparticle detection and sizing by mode splitting in an ultrahigh-q microresonator, Nat. Photon. **4**, 46 (2010).

[47] B. Peng, S. K. Özdemir, M. Liertzer, W. Chen, J. Kramer, H. Yilmaz, J. Wiersig, S. Rotter, and L. Yang, Chiral modes and directional lasing at exceptional points, Proc. Natl. Acad. Sci. USA **113**, 6845 (2016).

[48] C. Gmachl, F. Capasso, E. E. Narimanov, J. U. Nöckel, A. D. Stone, J. Faist, D. L. Sivco, and A. Y. Cho, High-power directional emission from microlasers with chaotic resonators, Science **280**, 1556 (1998).

[49] A. Brejnak, M. Gebski, A. K. Sokół, M. Marciniak, M. Wasiak, J. Muszalski, J. A. Lott, I. Fischer, and T. Czyszanowski, Boosting the output power of large-aperture lasers by breaking their circular symmetry, Optica **8**, 1167 (2021).

[50] K. G. Makris, A. Brandstötter, P. Ambichl, Z. H. Musslimani, and S. Rotter, Wave propagation through disordered media without backscattering and intensity variations, Light: Sci. Appl. **6**, e17035 (2017).

[51] A. F. Tzortzakakis, K. G. Makris, and E. N. Economou, Non-Hermitian disorder in two-dimensional optical lattices, Phys. Rev. B **101**, 014202 (2020).

[52] Q. Zhong, A. Hashemi, S. K. Özdemir, and R. El-Ganainy, Control of spontaneous emission dynamics in microcavities with chiral exceptional surfaces, Phys. Rev. Res. **3**, 013220 (2021).